ACS APPLIED MATERIALS & INTERFACES

Research Article

www.acsami.org

Organosilicon Coatings Deposited in Atmospheric Pressure Townsend Discharge for Gas Barrier Purpose: Effect of Substrate Temperature on Structure and Properties

Julien Petersen,[†,‡] Julien Bardon,*[,†] Aziz Dinia,[‡] David Ruch,[†] and Nicolas Gherardi*[,§,⊥]

[†]Advanced Materials & Structures, Centre de Recherche Public Henri Tudor, Rue de Luxembourg 66, L4221 Esch sur Alzette, Luxembourg

[‡]Institut de Physique et Chimie des Matériaux de Strasbourg (IPCMS) UMR 7504 CNRS-Université de Strasbourg, 23 rue du Lœss, BP 43, 67034 Strasbourg Cedex 2, France.

[§]Université de Toulouse, UPS, INPT, LAPLACE − Laboratoire Plasma et Conversion d'Energie, 118 route de Narbonne, 31062 Toulouse Cedex 9, France

[⊥]CNRS, LAPLACE, 31062 Toulouse, France

Supporting Information

ABSTRACT: Organosilicon plasma polymer and silicalike layers are deposited at different temperatures in a dielectric barrier discharge at atmospheric pressure operating in the Townsend regime. Final properties of these two kinds of layers can be finely tuned by the plasma process conditions. In particular, influence of deposition temperature is investigated when hexamethyldisiloxane based monolayers are deposited on poly(ethylene naphtalate) substrate. Coating chemical structure is tested by means of Fourier transform infrared spectroscopy and X-ray photoelectron spectroscopy. Their thickness, topography, and mechanical properties are evaluated by ellipsometry, scanning electron microscopy observation of coatings cross sections, atomic force microscopy, and nanoscratch testing. Permeability of coated polymer is measured for transparent silicalike layers, and the effect of coating structure on the oxygen gas permeability is discussed. The deposition temperature of coatings at 90 °C provides a strong improvement in barrier property compared to room temperature deposition, thanks to a densification of the SiO_2 matrix and to a decrease in the silanol group content.

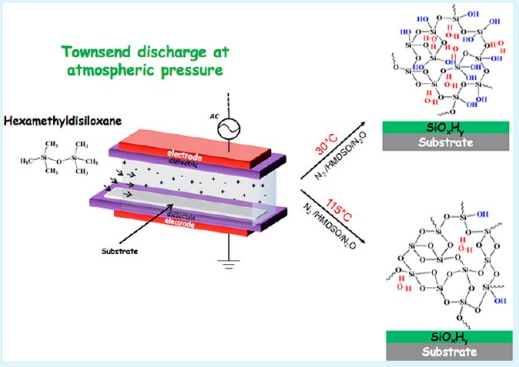

KEYWORDS: *dielectric barrier discharge, cold atmospheric pressure plasma, thin film coating, gas barrier layer, hexamethyldisiloxane*

1. INTRODUCTION

Organosilicon chemistry is promising for surface treatment purpose.[1] On the one hand, it generally involves harmless precursors and final products are recyclable. On the other hand, it is versatile because its chemistry can be tuned from an organic to an inorganic nature.[2,3] A challenge is to carry out deposition of organosilicon protective coatings on temperature-sensitive materials such as polymers. This can provide tribological protection on polymers,[4] antifogging properties[5] or an additional gas barrier protection on substrates such as poly(ethylene terephtalate) (PET) or poly(ethylene naphtalate) (PEN). In the latter case, organosilicon coatings can be involved in packaging applications[6] or encapsulation technologies for the protection of organic devices,[7] for instance, for light-emitting diodes (LEDs),[8] or in the frame of organic photovoltaic panels manufacturing.[9] Barrier performances corresponding to oxygen transmission rate (OTR) values better (lower) than 1×10^{-3} cm^3 m^{-2} day^{-1} are desirable for these encapsulation applications.

Plasma discharges at atmospheric pressure, when generated in a dielectric barrier discharge, are cold plasma, and therefore allow to deposit coatings on temperature sensitive substrates such as polymers.[10] Furthermore, they have the ability to coat large areas of polymer films at relatively high speed because no vacuum chambers are needed.[11] Such plasma processes are also versatile because they can be involved in substrate preparation treatment (otherwise called activation) and multilayer deposition.[12,13] Finally, deposition of plasma coatings with high gas barrier properties is reported at atmospheric pressure.[14]

A large number of studies investigates the influence of plasma parameters such as organosilicon and oxygen concentration in discharge,[15,16] plasma power,[15,17,18] working pressure,[16] influence of primer coating,[19] on barrier properties of obtained coatings. Further insights about the link between coating defects and gas barrier properties are given in an article from

Received: August 1, 2012
Accepted: October 8, 2012
Published: October 9, 2012

   dx.doi.org/10.1021/am3015229 | ACS Appl. Mater. Interfaces 2012, 4, 5872−5882

Leterrier.[20] In particular, defects of the SiO_x network at molecular level seem to be correlated to the concentration of silanol (Si−OH) groups within the coating.[6,17]

Previous studies[21,22] reported that these silanol groups density can be decreased by a further thermal post-treatment ("annealing") of the organosilicon plasma coating. Effect of surface temperature during PECVD of SiO_xH_y layer is studied in several articles.[23−29] Theses studies show the beneficial role of the substrate temperature in the densification of the SiO_2 matrix and the decrease of the film porosity. Moreover, Trunec and co-workers, which deposit such layer from an organosilicon monomer in a dielectric barrier discharge, report a decrease of the carbon and hydrogen content in the film when substrate temperature increases.[23] This could be related to the work of Deshmukh and Aydil,[30] which shows that during PECVD of SiO_2 below 100 °C, physically adsorbed organosilicon monomer can be trapped in the growing oxide giving rise to increased ethoxy and OH species which in turn adversely influence the coating integrity and quality. Hence, coatings deposited at higher temperature are expected to provide better barrier properties according to results from Schneider and co-workers.[6]

In this study, we report the deposition of organosilicon coatings on polyethylene naphtalate (PEN) for gas barrier purpose. The process is based on a dielectric barrier discharge reactor operating at atmospheric pressure (AP-DBD). The organosilicon precursor is hexamethydisiloxane (HMDSO). The plasma conditions and discharge configuration allow deposition in a homogeneous Townsend mode.[31] The effect of substrate temperature during deposition on the structural properties of coatings is particularly investigated.

2. EXPERIMENTAL SECTION

2.1. Atmospheric Pressure Plasma Deposition Process. Coatings are deposited in a dielectric barrier discharge. Experimental setup is sketched in the Supporting Information (Figure S1). The DBD is kept in a closed vessel to perform deposition experiments in a controlled atmosphere. The plasma reactor is slightly pumped down to 10^{-3} mBar before each deposition experiment, and then filled with nitrogen gas to reach atmospheric pressure. The DBD is ignited at atmospheric pressure between two parallel electrodes (5 cm wide × 2 cm long) made from metalized paint deposited on 635 μm thick alumina plates (see the Supporting Information, Figure S1).

A Vapor Source Controller (Bronkhorst company) delivers the target HMDSO flow rate at room temperature. A mixture of 10 ppm of gaseous HMDSO is diluted in a 3L/min N_2 flow and injected between the two alumina plates. Gentle pumping is performed during deposition to keep a constant pressure of 1 bar, thus continuously renewing the atmosphere in the discharge area. These conditions lead to deposition of a coating whose composition is described as polydimethyldisiloxane-like (PDMS-like) with nitrogen-containing moieties, or $SiO_xC_yN_zH_w$.

When nitrous oxide (N_2O) is added as an oxidizing gas, it leads to an inorganic coating whose composition is described as hydroxylated silicalike, or SiO_xH_y. 240 ppm of N_2O is added to the mixture so that stoichiometric ratio to form SiO_2 from HMDSO and N_2O is targeted. In fact, previous studies have shown that for all N_2O-to-HMDSO ratios larger than 12, completely inorganic films are deposited with no significant discrepancies in the O-to-Si ratio in the layer.[31,32] To get a homogeneous discharge in N_2 as a carrier gas (called a Townsend discharge), the gas gap is set to 1 mm, and the discharge is driven by AC high-voltage of 13 kV peak to peak at a frequency of 3 kHz, which corresponds to a discharge power of 0.5 W/cm^2. More details about the reactor can be found elsewhere.[5]

A heating device with a temperature closed loop control is inserted into the bottom electrode, close to the substrate. A target temperature is set for every deposition experiment. Substrate temperature is measured with an optical pyrometer (Ecom instruments) for a given target temperature.

Deposition is performed on poly(ethylenenaphtalate) (PEN) and silicon substrates. First, coatings are deposited in static mode (no displacement of the substrate) on silicon (Si) wafers. These wafers are cleaned before deposition experiments in piranha solution (3:1 concentrated sulfuric acid to 30% hydrogen peroxide solution) for 10 min and rinsed in demineralized water and then in hydrofluoric acid for 10 min. Finally, they are rinsed again in demineralized water prior to the deposition process.

Coatings are also deposited on 65 mm wide and 50 μm thick PEN films purchased from Goodfellow. The reactor is equipped with a roll-to-roll foil transport system which allows obtaining homogeneous coatings on length greater than the electrode length (2 cm). In this case, deposition experiments are performed on length greater than 5 cm to get samples which have suitable dimensions for gas permeability testing (5 × 5 cm^2). The gases for the AP-DBD process are nitrogen (99.998% purity) and nitrous oxide (99.998% purity) purchased from Air Liquide (Toulouse, France). The monomer hexamethyldisiloxane (HMDSO, NMR grade with purity ≥99.5%) is purchased from Aldrich.

2.2. Characterization of Coatings. FTIR spectroscopy is performed with a Biorad FTS 80A spectrometer in transmission mode on Si wafer substrates. Spectra are recorded in the range 500−4000 cm^{-1} with a 4 cm^{-1} resolution. Further peak decomposition is performed with Casa XPS software, assuming purely Gaussian peaks.

Surface chemical compositions of coatings are investigated by X-ray photoelectron spectroscopy (Hemispherical Energy Analyzer SPECS, PHOIBOS 150) by means of a monochromatic Al K radiation operating at 200 W with an anode voltage of 12 kV. No etching step is performed prior to the analysis on the PDMS-like coatings. As for silicalike coatings, a slight etching step is performed with an Ar^+ ion beam of 500 eV energy and 60 μA/cm^2 current density at an incident angle of 45° for 30 s. The pressure in the analysis chamber is 1×10^{-9} mbar. XPS spectra are referenced with respect to the C 1s peak at 284.6 eV originating from carbon contamination. Core peaks are analyzed using a nonlinear Shirley-type background and fitted using 70% Gaussian, 30% Lorentzian lineshapes with Casa XPS software.

Coatings thickness is evaluated using spectroscopic ellipsometry. Coatings are assumed to be homogeneous and isotropic. Measurements on SiO_xH_y coatings are carried out with a Sopra GES 5 spectroscopic ellipsometer in a spectral range from 250 to 750 nm. Beam size and angle of incidence are set to (0.1 × 0.5) mm^2 and 75°, respectively. As for $SiO_xC_yN_zH_w$ coatings, measurements are performed with a spectroscopic ellipsometer AutoSE from Horiba Scientific in a spectral range from 450 nm and 1000 nm, and with a constant angle of incidence of 70°. Curves giving the ellipsometric angles ψ and Δ as a function of wavelength allows calculating the film thickness using a double layer model. First layer is a semi-infinite silicon substrate and second layer is the plasma coating. In case of SiO_xH_y coatings, second layer is modeled according to a Bruggemann effective medium approximation. The layer is actually considered as a mixture of a-SiO_2 and void. In the case of PDMS-like coatings, a dispersion law is used. Thicknesses given here are averaged (±one standard deviation) over 3 measurements performed along the width of silicon wafer substrate. The validity of ellipsometry results has been checked for both types of coatings by measuring thickness of a few layers with a 2D profilometer (Alphastep IQ from KLA Tencor).

$SiO_xC_yN_zH_w$ coatings structure is determined by scanning electron microscope (SEM) on cross-section of coatings deposited on Si wafers. Observations are carried out with a QUANTA 200 FEG from FEI Company. This microscope is a Variable Pressure SEM (VP-SEM) that is able to observe insulating samples directly without any additional metallization.

The topography of plasma coatings is evaluated by atomic force microscopy (AFM) with a PicoSPM LE from Scientec. AFM experiments are carried out with silicon nitride cantilevers (Park Scientific) in tapping mode.

Scratch test experiments are carried out on SiO_xH_y coatings deposited on polymers with a CSEM nanoscratch tester apparatus (reference NST-S-AE-0000). Scratching tip is a conosphere having 90° apex and a 10 μm radius of curvature. It is made from high-speed steel coated with diamond like carbon. Fracture resistance of the different coatings are evaluated by scratch experiments performed with an increasing normal load from 0.1 mN to 40 mN for a 0.4 mm long scratch. Scratch speed is 0.5 mm/min. Series of two or three scratches are performed on the coated sample at two different locations to evaluate reproducibility of the method. Each scratch residual track is observed with optical microscopy coupled to the scratch apparatus. First occurrence of a damage is detected and the corresponding critical load is recorded.

Dynamic mechanical analysis (DMA) is carried out on PEN substrate with a DMA equipment 242C from Netzsch. Dimensions of rectangular film samples are 10 mm × 5 mm with a 500 μm thickness. Tests are performed in tensile testing configuration from 20 to 180 °C with a heating rate of 2 °C/min. The static and dynamic load is set to 0.2 and 7 N, respectively. Scanning frequencies are 1, 5, and 20 Hz.

The coating permeability to oxygen is tested with a Mocon OxTran 2.61 permeameter at 90% relative humidity (RH) and 25 °C. Since gas barrier properties are targeted, 100 nm thick inorganic monolayers are deposited on the PEN substrate. Indeed, previous work shows that a minimum thickness of 50 nm shall be deposited for this purpose.[13] Stabilization of the permeability value is reached after a transitory regime, which last typically 60−80 h. A measurement point is recorded every 5 h. Characteristic value of the sample is assumed to be the last measured value. An indicative value of measurement deviation on a given sample is provided by calculating the standard deviation of the three last recorded values.

3. RESULTS AND DISCUSSION

3.1. Deposition Rate. In this work, effect of substrate temperature is evaluated on two kinds of films deposited from HMDSO, namely PDMS-like ($SiO_xC_yN_zH_w$) and silicalike (SiO_xH_y), respectively obtained without and with N_2O in the gas mixture. First, deposition rates are measured at different substrate temperatures. Coatings are deposited on Si wafers in static mode and deposition rates are evaluated by ellipsometry. Corresponding results are represented in Figure 1.

Gas mixture, including HMDSO precursor, is injected longitudinally in the inlet of the plasma area (position = 0 mm at the inlet). Hence, the variations in the deposition rate profile as a function of the distance from the inlet give information on precursor consumption and on growth mechanisms.[32,33] Panels a and b in Figure 1 provide the deposition rate profile of $SiO_xC_yN_zH_w$ and SiO_xH_y coatings, respectively. Close to room temperature (30 °C), deposition rate tends to increase as a function of distance in the case of $SiO_xC_yN_zH_w$ layers, whereas it tends to decrease as a function of distance in the case of SiO_xH_y layers.

These growth rate profiles have to be discussed with reference to the chemical composition of the coatings. Concerning SiO_xH_y layers, XPS analysis shows that elemental composition does not change according to the distance from the inlet (Table 1), which is in accordance with previous studies done in similar experimental conditions.[13,31] Therefore, the shape of the thickness profile mainly comes from precursor consumption along the electrode, as it has been shown previously through numerical simulations.[32,33]

Concerning $SiO_xC_yN_zH_w$ layers, at 30 °C temperature, its composition changes with the distance (Table 1), which is again in accordance with other studies.[13,31,34] On the one hand, the decrease of the silicon and oxygen concentrations along the gas flow has to be related to the precursor depletion, which occurs similarly to the silicalike case. On the other hand,

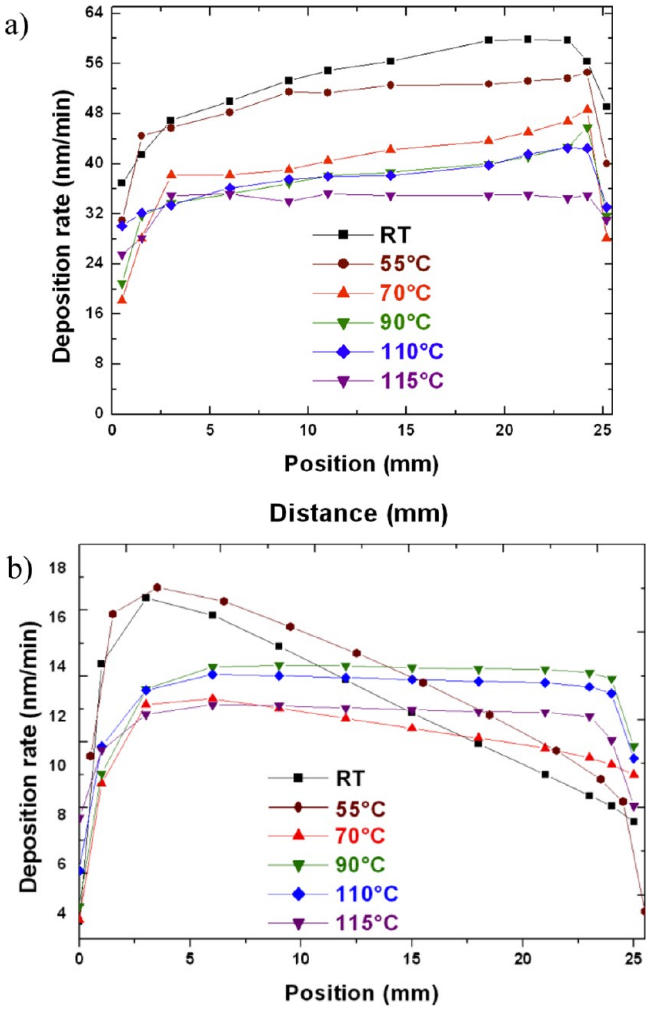

Figure 1. Deposition rate profile of (a) PDMS-like and (b) silicalike coatings at different temperature. For these particular measurements, deposition experiments are performed in static mode (no roll-to-roll movement) on a silicon wafer.

Table 1. XPS Elemental Composition of Thin Films As a Function of the Position

type of coatings	position	%Si	%O	%C	%N	O/Si
silicalike @ 30 °C	entrance	30.2	67.8	1.6	0.4	2.24
	exit	30.2	68	1.5	0.3	2.25
PDMS-like @ 30 °C	entrance	35	21	25.5	18.5	0.6
	exit	27.5	17.5	32	23	0.6
PDMS-like @ 115 °C	entrance	52.1	28.3	18.4	1.2	0.54

because of the fact that no additional oxygen species is added in the gas phase, the carbon and nitrogen concentrations increase along the gas flow because of the deposition of organic byproducts remaining and accumulating in the gas.[13] Thus the increase in the deposition rate as a function of distance is assumed to come from the deposition of these organic byproducts.

In both cases ($SiO_xC_yN_zH_w$ and SiO_xH_y layers), thickness homogeneity on the whole distance is improved when temperature increases. For PDMS-like coatings, the deposition rate decreases whatever the position: the average deposition rate decreases from 50 nm/min at 30 °C to 32 nm/min at 115 °C. This is due to the fact that a greater quantity of the organic

dx.doi.org/10.1021/am3015229 | ACS Appl. Mater. Interfaces 2012, 4, 5872−5882

byproducts are released from the coating and not redeposited when temperature increases. Hence, when the substrate temperature is changed from 30 to 115 °C, the concentration of Si in the coating increases when the one of C decreases (Table 1). Because the contribution of the organic byproducts to the growth rate profile is maximum at the exit of the discharge (where their concentration is the highest), the decrease of the growth rate when the temperature increases is more important at the exit than at the entrance, resulting in a flatter profile.

On the contrary, for silicalike coatings, the average growth rate is very close to 14 nm/min whatever the deposition temperature is: only the shape of the growth rate profile is influenced by the temperature. The growth rate actually decreases at the entrance of the discharge and increases at its exit. It is generally assumed that an increase of the substrate temperature leads to higher surface mobility and higher desorption coefficient (or lower sticking coefficient).[35] This may explain the higher homogeneity as a function of distance observed at high temperature. Indeed, we already mentioned that at room temperature, the shape of the growth rate comes from the precursor consumption along the electrode. If the sticking coefficient decreases, this results in a slower decrease of the precursor concentration in the gas phase, and therefore to a higher growth rate for longer residence times, i.e., larger distances from the inlet.

3.2. Structural Properties of $SiO_xC_yN_zH_w$ Coatings.

First, the molecular structure of $SiO_xC_yN_zH_w$ coatings deposited under N_2/HMDSO plasma is studied according to the substrate temperature. FTIR measurements of coatings deposited on silicon wafers are performed in transmission mode (Figure 2). Corresponding assignment of peaks is provided in Table 2. FTIR spectra are recorded for every deposition temperature and their amplitude is normalized so that each spectrum has the same maximum amplitude for the intense peak appearing at 1040 cm^{-1}. Coatings are always analyzed at the same position, namely in the center of the sample (i.e., 10 mm from the gas inlet) in order to not be influenced by the variation of chemical composition observed along the gas flow. Coating deposited at room temperature exhibits a structure close to PDMS and a high contribution of nitrogen-containing bonds is detected. Several functional groups such as hydroxyl, carbonyl or amine groups are assumed to come from interactions of precursor and carrier gas with activated species from the plasma. Methyl groups are identified at 2959 and 2923 cm^{-1}. At low wavenumbers, FTIR spectrum shows the fingerprint of organosilicons. Bands at 804, 840, and 1267 cm^{-1} are characteristic of $Si(CH_3)_2$, $Si(CH_3)_3$ and $Si(CH_3)_x$ functional groups, respectively. In the case of $SiO_xH_yC_z$ coatings, the intense band between 1020 and 1250 cm^{-1} is related to Si−O−Si and Si−O−C asymmetric stretching modes. More precisely, it can be decomposed as the sum of three Gaussian contributions (see the Supporting Information, Figure S2) at 1120, 1070, and 1030 cm^{-1} related to different bond characteristics, such as bond angle and length.[27,36−38] In amorphous SiO_2, these 3 bands would be associated with 170−180° (TO_2 mode), 140° (TO_1 mode), and 120° (TO_3 mode) Si−O−Si bond angles, respectively.[36,37] The TO_1 mode reflects a quartz-like structure in a fold ring configuration. TO_2 mode is often associated to fragments of Si−O−Si chains, but due to the strong concentration of carbon in the films, one cannot exclude here that this mode is perturbed by the Si−O−C stretching modes appearing in the same wavenumbers range (1100−1180 cm^{-1}).[39] When considering SiO_2, TO_3 mode has to be related to planar 3-fold rings or packed 4-fold rings (coesitelike structure).[36,27] However, in the case of a $SiO_xC_yH_z$ coating, such low Si−O−Si bond angle is often observed because of the methyl environment of the bond. Indeed, the angle of the Si−O−Si bond angle is close to 120° when Si−O−Si is submitted to repulsion forces from electrons pairs (in bonds of H or methyl groups attached to Si in X_2−Si-O_2 (X═H, CH_3)), as in solixane structures.[38] Actually, this is this contribution which dominates the asymmetric stretching mode (see the Supporting Information, Figure S2).

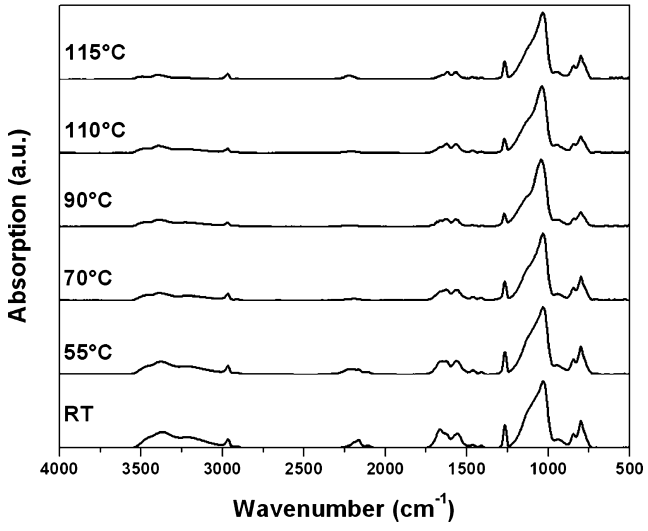

Figure 2. FTIR spectra of $SiO_xC_yN_zH_w$ coatings deposited at different temperatures.

Table 2. Assignment of FTIR Peaks[a]

chemical bonding	vibration mode[b]	functional group	wavenumber (cm^{-1})
Si−O	ν_s	Si−O−Si	790−830
	ν_{as}	Si−O−Si	1030−1210
	ν_s	Si−O−CH_3	840
	ν_{as}	Si−O−CH_3	1132
Si−C	ν	Si−$(CH_3)_2$	804
	ν_s	Si−$(CH_3)_x$	1267
Si−H	ν		2180
CH	ν_{as}	CH_2	2908
	ν_{as}	CH_3	2966
C═N	ν	amide I	1666
C═O	ν	amide II	1640
		−C═O	1413
C≡N	ν		2221
NH	ν	amine	3190
NH_2	ν	amide	3388
OH	δ	SiOH	940−950
	ν	H_2O	3350
	ν	SiOH	3515
		SiOH	3640

[a] $SiO_xC_yN_zH_w$ coatings are concerned with the whole set of functions. SiO_xH_y coatings are only concerned by underlined bands. [b] δ: bending mode; ν: stretching mode; s: symmetric; as: asymmetric.

dx.doi.org/10.1021/am3015229 | ACS Appl. Mater. Interfaces 2012, 4, 5872−5882

When substrate temperature increases, a decrease in carbon functional groups such as amines, amides, or organosilicon groups is observed, as well as a modification of the backbone band shape. As previously discussed in the deposition rate section, it is assumed that increasing the substrate temperature eliminates the chemical groups, which are not thermally stable such as hydroxyl and amino groups. However, at 115 °C, the presence of amide and nitrile groups, which are more stable, is still observed. Concerning the silicon containing bonds, the increase in the temperature leads to a decrease of the amplitude of the peaks related to the $SiCH_3$ group peaks amplitude and to a decrease of the contribution located at 1125 cm^{-1} attributed to the fragments of Si−O−Si chains and/or to Si−O−C bond (see the Supporting Information, Figure S2). These results predict a decreasing porosity[40] of the film according to the temperature which should be due to an increase of the cross-linking. This will be further confirmed by SEM images (see below).

Figure 3 provides the elemental composition determined by XPS of $SiO_xC_yN_zH_w$ coatings as a function of substrate temperature. As already briefly discussed in section 3.1, it is observed that oxygen and silicon content increases when substrate temperature increases, whereas carbon and nitrogen incorporation in the coating decreases. Additional information about the coating structure is provided by C1s peak decomposition. The spectra is fitted into six components corresponding to, C−H at 283.5 eV, Si−C at 284.6 eV, C−O at 286 eV, C−N at 287 eV, N−C═O at 288.5 eV, and O−C═O at 289.3 eV. Results of such decomposition are illustrated for coatings deposited at 30 and 115 °C in the Supporting Information (Figure S3). A strong decrease of nitrogen and oxygen containing groups is observed. This is consistent with the FTIR results and with the variation of the elemental composition which changes from $Si_2O_{1.25}C_{1.5}N$ at 30 °C to $Si_2OC_{0.6}N_{0.07}$ at 115 °C (to be compared with the elemental composition of HMDSO: Si_2OC_6). It confirms that when the temperature is increased, the backbone of HMDSO molecule (Si−O−Si bond) is maintained, whereas the thermally unstable organic groups are eliminated during the growth.

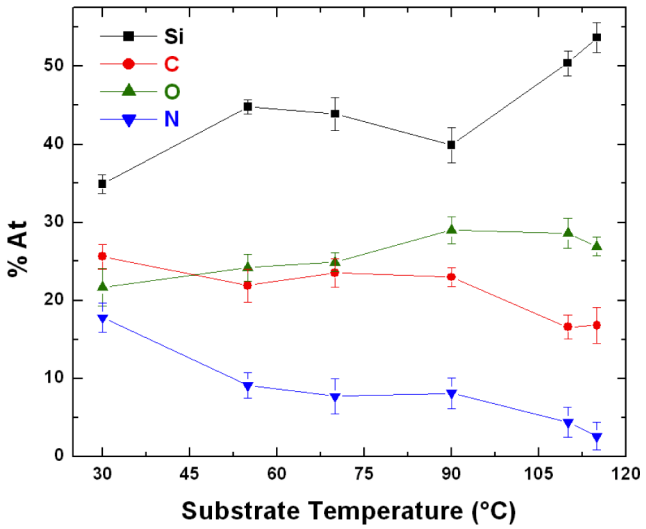

Figure 3. Elemental composition of $SiO_xC_yN_zH_w$ coatings as a function of deposition temperature.

Coating microstructure is observed by SEM on cross-sections when the coating is deposited on wafers. Pictures of coatings deposited at different temperatures are shown in Figure 4. At low substrate temperature (<90 °C), coatings show a columnar structure. This comes together with a high porosity. When temperature increases, SEM observations reveal smoother coatings and a more compact structure, which is in accordance with a better diffusion of precursor molecules and molecules fragments in the plasma and on the surface. This leads to a better homogeneity. It is otherwise observed that deposition rate decreases, as discussed previously. These observations can be directly correlated with FTIR and XPS results from which one could expect that the film is more cross-linked when the substrate temperature increases.

Additional information to SEM analysis is given by AFM measurements on the coating surface. AFM pictures performed on the coatings deposited at different temperatures are given in Figure 5a. AFM pictures are consistent with SEM cross-section as smoother topography is observed when temperature increases. Topography smooth structure seems to come qualitatively from finer peaks, i.e., peaks in-plane area decreases as a function of temperature. Corresponding roughness is given in Figure 5b. Roughness amplitude decreases strongly as temperature increases, to reach RMS value around 1 nm at 115 °C. Therefore, both SEM and AFM observations leads to

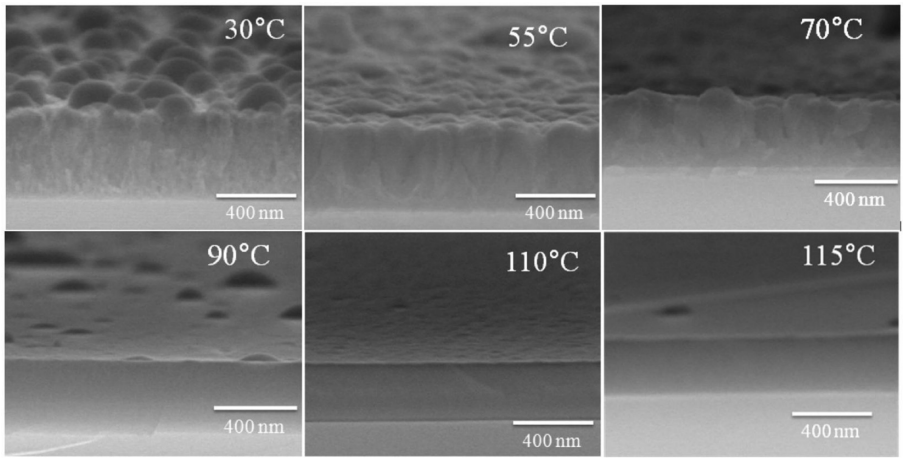

Figure 4. SEM pictures of coatings cross-sections. Coatings are deposited at 6 different temperatures (see captions).

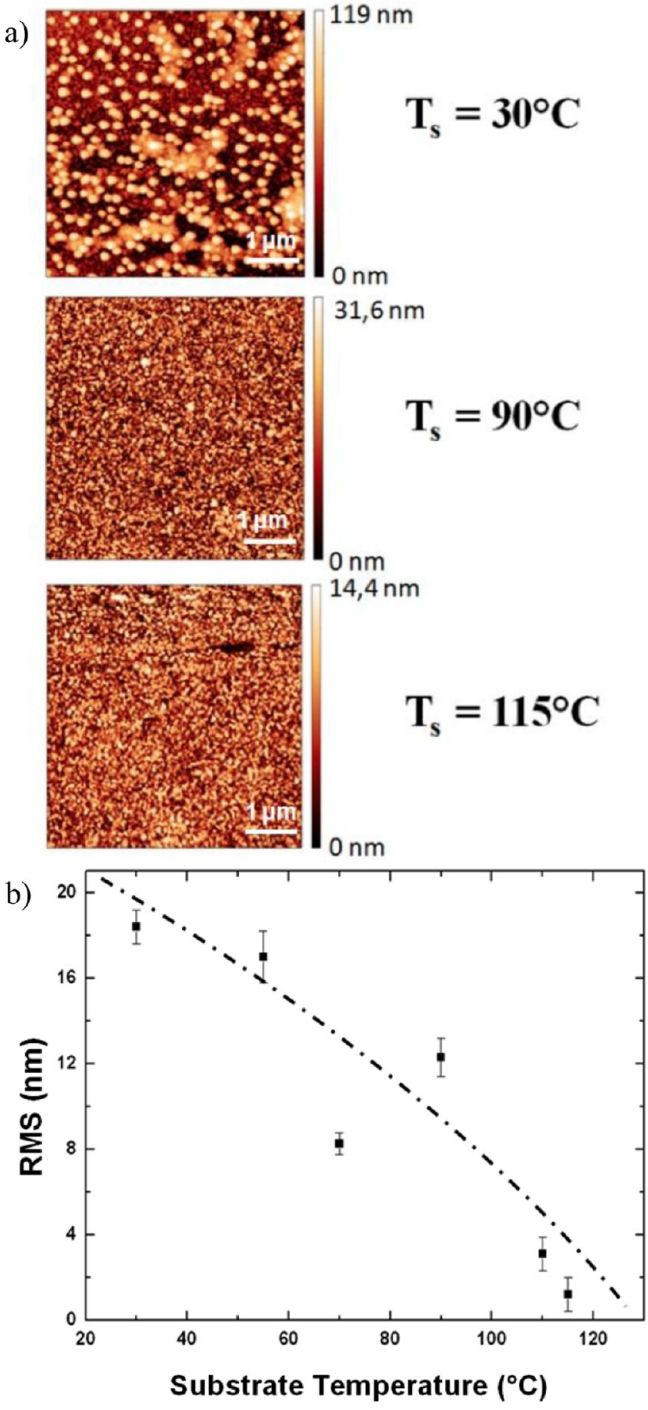

Figure 5. (a) AFM pictures of coatings performed at different temperatures (5 × 5 μm area, 400 nm thick coatings). Height scale is not standardized. (b) RMS roughness value as a function of temperature.

assume an increase of the diffusion on the surface and a decrease of the sticking coefficient (or an increase of the reemission) when temperature increases; indeed, surface morphology generally changes from a columnar-like structure to a smooth morphology as the sticking coefficient is decreased.[41]

As a conclusion, increasing the deposition temperature for HMDSO based coatings deposited in a Townsend discharge leads to coatings with a more homogeneous and finer structure. Chemical composition also changes as a function of temperature and becomes more inorganic and cross-linked.

3.3. Structure and Properties of SiO_xH_y Coatings. The addition of N_2O during plasma process leads to an inorganic surface with no incorporation of nitrogen, as detected by XPS, and with a carbon concentration detected in the bulk around 1.5% (Table 1). Close to room temperature, the silicalike material has a stoichiometric ratio (O/Si) equals to 2.24. It can be pointed out here that the same stoichiometric ratio has been measured on coatings deposited in the same plasma conditions but on a polymer substrate,[5] showing that at least from a chemical point of view the films deposited on c-Si and on polymer are similar. In this study, the influence of the temperature increase on the SiO_xH_y coatings has been investigated by FTIR analyses. FTIR spectra of the coatings are given in Figure 6 and peak assignment is summarized in Table 2 (underlined bands).

Figure 6 also present the evolution according to the temperature of the main −OH band centered at 3400 cm^{-1} (Figure 6b) and of the Si−O−Si asymmetric stretching band centered at 1060 cm^{-1} together with the SiOH valence vibration at 930 cm^{-1} (Figure 6c).

As observed in Figure 6b, the area of the main hydroxyl band found between 2900 and 3750 cm^{-1} decreases strongly when the substrate temperature increases. Its shape proceeds from at least the three contributions following in order to be satisfactory reproduced: (1) the presence of isolated and germinal (two hydroxyls on the same Si atom) Si−OH groups trapped into the matrix, noted as free Si−OH in the following; (2) the presence of vicinal (two hydroxyl groups on two neighboring Si atoms) Si−OH groups interacting between them, noted as H-bonded Si−OH in the following; (3) the presence of free and H-bonded molecular water embedded into the matrix.[23,42,43]

The free Si−OH groups trapped into the matrix give a clear absorption observed around 3640 cm^{-1}.[23,28,42−47] One can note here that free Si−OH surface groups, normally found as a narrow absorption peak around 3750 cm^{-1},[23,47] are not found in our spectra. The position of the absorptions peaks related to the H-bonded Si−OH groups and to the water molecules is more controversial. Most of the studies agree that the H-bonded Si−OH groups give absorption at frequency ranging from 3500 to 3650 cm^{-1} depending on their mutual interaction strength, the free and H-bonded water molecules contributing to the 3210−3425 cm^{-1} range.[23,43,46] Also, a red shift (toward lower wavenumbers) of the central position of the −OH main band is generally attributed to a higher appearance of hydrogen bridged bonds.[28,44] However, some discrepancies can be found, some authors positioning the H-bonded Si−OH around 3450 cm^{-1} (the H−OH stretching band of H_2O being at 3230 cm^{-1}),[42,45] a few others positioning it at even lower wavenumbers (3200 cm^{-1}), the water vibrations being seen in this last case around 3400 cm^{-1}.[28] The hydroxyl band is therefore split up in three contributions: a band centered at 3300 cm^{-1}, which is assigned to molecular O−H groups present in water, a band centered at 3515 cm^{-1} linked to H-bonded Si−OH groups, and a band located at 3640 cm^{-1}, which comes from free Si−OH groups into the matrix. Of course, this analysis is not unique but presents the advantage of being suitable for all our samples. An example of such decomposition can be seen in the Supporting Information (Figure S4a). The evolution of the respective area of these three contributions (Figure 6b and the Supporting Information,

dx.doi.org/10.1021/am3015229 | ACS Appl. Mater. Interfaces 2012, 4, 5872−5882

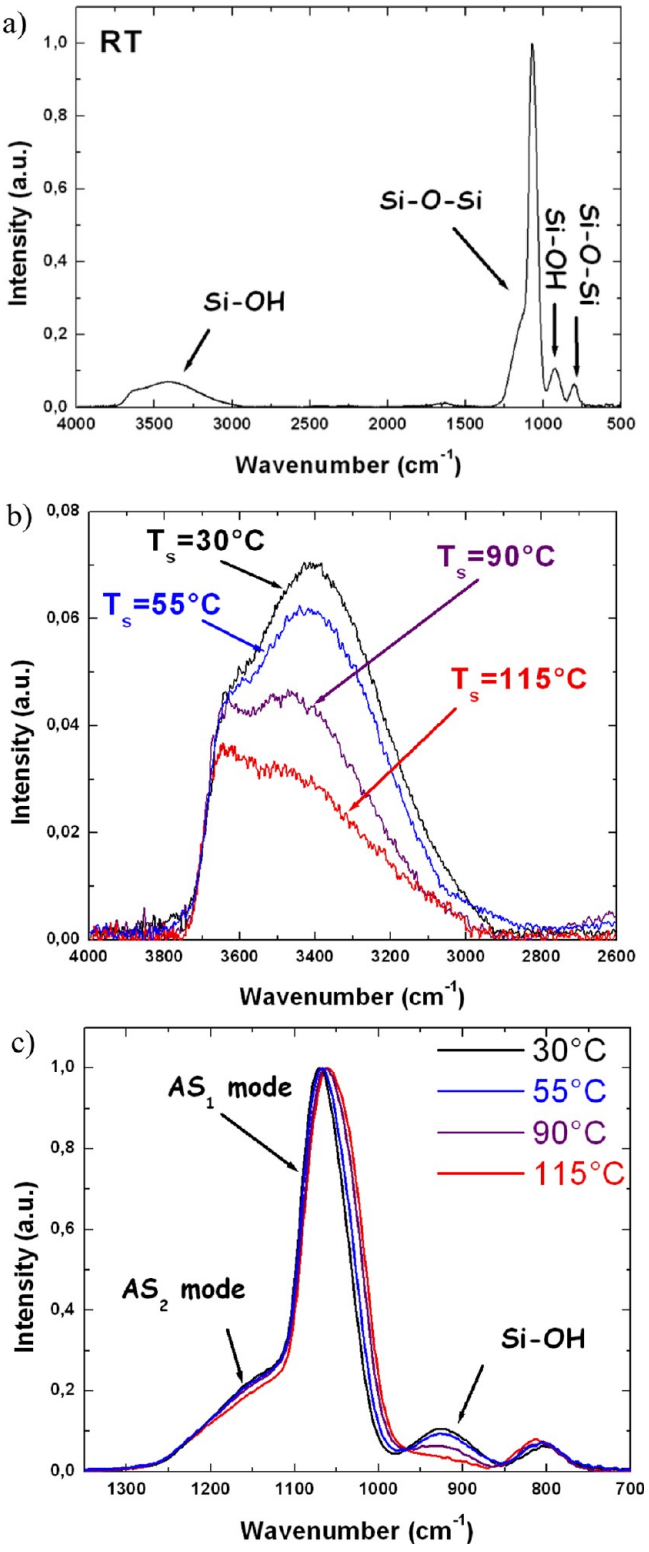

Figure 6. FTIR spectra of monolayer silicalike coatings obtained at different temperatures (a) general spectra obtained at 30 °C (b) hydroxyl groups (c) Si−O−Si backbone.

Figure S4b) shows clearly that the free Si−OH one barely changes with temperature. On the other hand, these are the areas of the two other contributions (bonded Si−OH and H−OH) which strongly decrease when deposition is performed at high temperature. As a result, the central position of the whole −OH band is shifted from 3410 cm^{-1} to 3500 cm^{-1}, which indicates a lower appearance of H-bridged bonds. As it can be seen in Figure 6c, this evolution is associated to a strong decrease of the amplitude of the Si−OH band located at 930 cm^{-1}. This confirms that the decrease has to be linked to a lower concentration of the −OH groups when the temperature increases, and is not due to a geometrical separation of hydroxyl groups as observed for example in ref.[28]

The analysis of the asymmetric stretching band (Figure 6c) can give information about the effect of the substrate temperature on the Si−O network.[48] This band can be decomposed as the sum of two Gaussian peaks (see the Supporting Information, Figure S5): AS_1, the most intense peak, also referenced as TO_1, is located at 1070 cm^{-1}, and is assigned to the in-phase asymmetric stretching vibrational mode of the neighboring SiO_2 moieties (−O−Si−O−) in a quartzlike structure; its 180° out-of-phase counterpart (AS_2) is located in the shoulder left, around 1140 cm^{-1}.[49] The ratio between these two bands is assigned to the disorder in the structure of the film.[27,40] Indeed, the AS_2 mode reflects the existence of fragments of Si−O−Si chains, or the presence of local structures with ∼170−180° Si−O−Si bond angles, like in the β-cristobalite polymorph of the crystalline silica.[27] Note that the TO_3 vibration band at ∼1030 cm^{-1} is not detected in these coatings.

Figure 7 displays the position of the AS_1 peak maximum and the AS_1/AS_2 area ratio according to the substrate temperature.

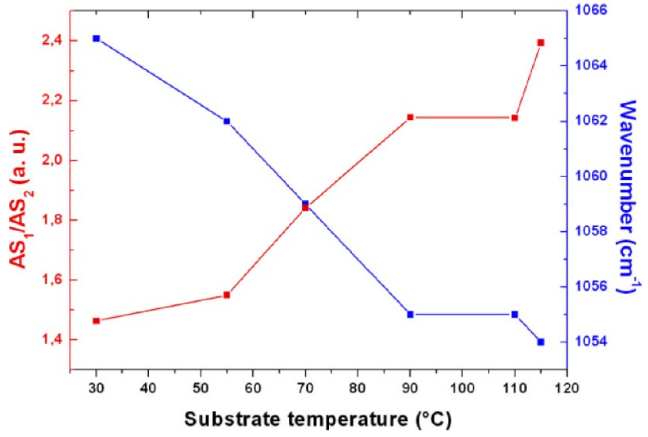

Figure 7. Area ratio of two peaks linked to Si−O−Si stretching and position of more intense peak as a function of temperature.

At room temperature, the position of AS_1 peak maximum is around 1066 cm^{-1}. This value is lower than for the thermal silica (1078 cm^{-1}), indicating a smaller angle Si−O−Si which, in our case, is assumed to come from the presence of Si−OH and/or nitrogen and carbon elements in very low concentrations.[45,49] However, and surprisingly, the AS_1 peak is red-shifted when the temperature increases. At first, a blue shift had been expected, to approach the value of the thermal silica. However, this phenomenon can be explained otherwise by the modification in the environment around the Si−O bond triggered by the removal of the hydroxyl groups. Indeed, as silicon atom replaces a hydrogen atom which is lighter, the oscillation of the Si−O bond is shifted to a lower frequency. Moreover, Landreau et al. have shown that a red shift of this peak is associated with a decrease in the stoichiometric ratio x in SiO_x,[28] which is larger than 2.2 at room temperature in our case (Table 1). Thus, a decrease in this ratio is consistent with

dx.doi.org/10.1021/am3015229 | ACS Appl. Mater. Interfaces 2012, 4, 5872−5882

the decrease in the OH groups content discussed previously. As for the AS_1/AS_2 ratio, it increases from 1.46 to 2.4 when the temperature increases, indicating an increase of the cross-linking,[28] a decrease in the porosity,[40] and an increase in the density of the coating network.[45,50] These results suggests that coatings deposited at higher temperature should exhibit better gas barrier properties.

AFM pictures demonstrate that SiO_xH_y coating surface is very flat (see the Supporting Information, Figure S6). RMS roughness amplitude values calculated on 5 × 5 μm pictures slightly decrease from 0.95 nm for the coating deposited at 30 °C to 0.41 nm at 90 °C and 0.37 nm at 115 °C, probably because of the increase in the surface mobility at higher temperature. These values have to be compared with the roughness value for the substrate (silicon wafer) which is around 0.2 nm. In this case, roughness amplitude values from the coatings and from the substrate are close, which is also observed by Premkumar et al. for PEN substrate.[14]

These significant changes in SiO_xH_y coatings structure must have a significant influence on coatings mechanical properties. Therefore, mechanical properties of SiO_xH_y coatings deposited on PEN substrate are tested by nanoscratch. Observation of residual scratch tracks is performed and damages are identified (cracking, spaling, perforation, among others). Qualitative analysis of scratch micrographies show that damages observed as normal load increase are similar whatever the deposition temperature. However, first occurrence of a damage which is identified as lateral spalliation (see the Supporting Information, Figure S7) is detected for different loads for coatings deposited at different temperatures. Corresponding values are given in Figure 8.

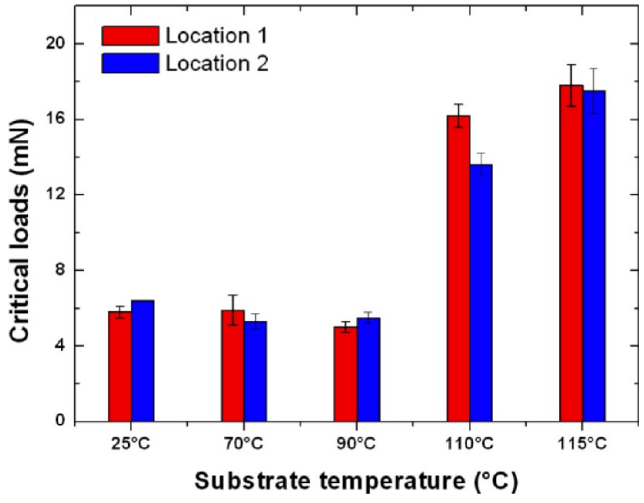

Figure 8. Critical load for lateral spalliation measured on two different series of scratches for each deposition temperature.

Lateral scales are observed together with forward cracks inside the scratch track. Both damages are related to the coating failure. Therefore, they provide comparative information when critical loads are compared between different coatings, i.e., when deposition temperature increases. Critical load for lateral spalliation significantly increases for temperature higher than 110 °C.

Internal stress within the coating may be responsible for a change of critical load as a function of temperature. It comes from two parts, as already described in the article from Leterrier.[20]

First, temperature change from deposition temperature to room temperature is responsible for thermal stress σ_t. Formula 2 in ref 20 is given as eq 1.

$$\sigma_t = \frac{E_c}{1-\mu_c}\int_{T_i}^{T_f}\{\alpha_S(T) - \alpha_c(T)\}dT \quad (1)$$

where E_c, μ_c, and α_c are, respectively, the Young modulus, Poisson coefficient, and linear thermal expansion coefficient of the coating, α_s is the linear thermal expansion coefficient of the substrate, and T_i and T_f are initial and final temperatures, respectively.

Calculations from eq 1 show that in the case of our experiments, the thermal stress is compressive in the coating and its value should be in the range 0 to 150 MPa, which is small when strength of fused silica is considered (several GPa). Furthermore, critical loads are linked here to forward crack damaging, which is triggered by compressive load forward and under the tip during scratch movement. An increase in thermal stress is responsible for an increased compression stress in the layer, which makes the coating more sensitive to an additional compressive stress, and thus less resistant to scratch. This is not observed here; therefore, this thermal stress contribution is certainly not responsible for a change in critical load.

Second, defects in the micro/nanostructure of silicalike layers are responsible for intrinsic stress, and are also related to the mechanical resistance of the coating. FTIR analyses of silanol groups and AFM measurements have shown that the coating heterogeneity and defects in the silica network tend to decrease when deposition temperature increases. Therefore, this better quality silica coating obtained at high temperature probably explains the higher critical loads recorded for scratch testing.

An additional effect could be the fact that an increased deposition temperature may lead to a better adhesion between PEN and silicalike layer. Indeed, an increased deposition temperature triggers evaporation of water which is entrapped in the thermoplastic polymer substrate.[51]

Oxygen transmission rate (OTR) results for coatings deposited at different temperatures are given in Figure 9. As

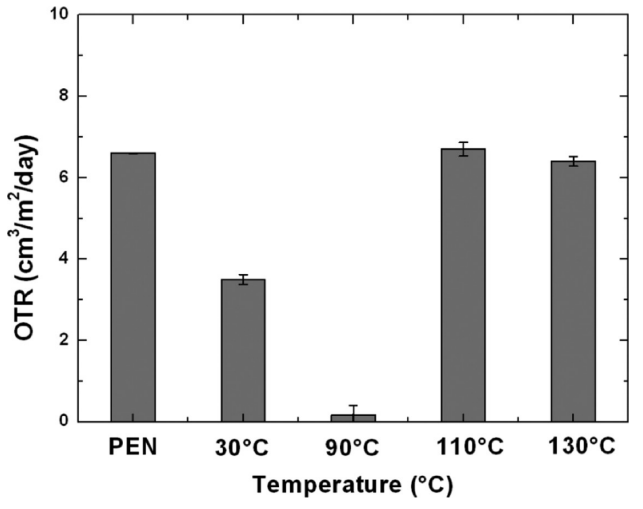

Figure 9. OTR (oxygen transmission rate) obtained for PEN coated with silicalike monolayer coatings (100 nm thick) performed at different temperatures.

dx.doi.org/10.1021/am3015229 | ACS Appl. Mater. Interfaces 2012, 4, 5872−5882

expected, permeability decreases, i.e., barrier property increases, when deposition temperature increases, to reach the lowest value of 0.2 cm^3 m^{-2} day^{-1} at 90 °C. This OTR value corresponds to a barrier improvement factor (BIF) of 33, which is high enough to address the majority of packaging applications.[9]

Apart from the very high performances obtained by Premkumar et al.[14] from atmospheric pressure air or nitrogen discharges with argon and HMDSO or tetraethylorthosilicate (TEOS) admixtures, this value is in very good accordance with other values obtained for a silicalike monolayer deposited by low-pressure PECVD,[16,52−54] showing the good quality of the layers deposited in this work.

According to articles,[6,16] lowering the concentration of OH groups within the coating leads to better oxygen barrier properties, which is consistent with the results presented here where OH concentration tends to decrease when deposition temperature increases.

However, no barrier property is provided by the coating when deposition temperature is above 110 °C. This is typically the case when cracking occurs in the layer. Optical microscope observation actually shows regular cracks in the silica layer for the coatings deposited above 110 °C (shown in Figure 10a), which is consistent with these results.

Cracking at high temperature in the silica layer may be due to stretching of PEN substrate during deposition. Actually, roll-to-roll system allows moving the PEN film for deposition on a larger span, but also applies a significant tensile load to the film.

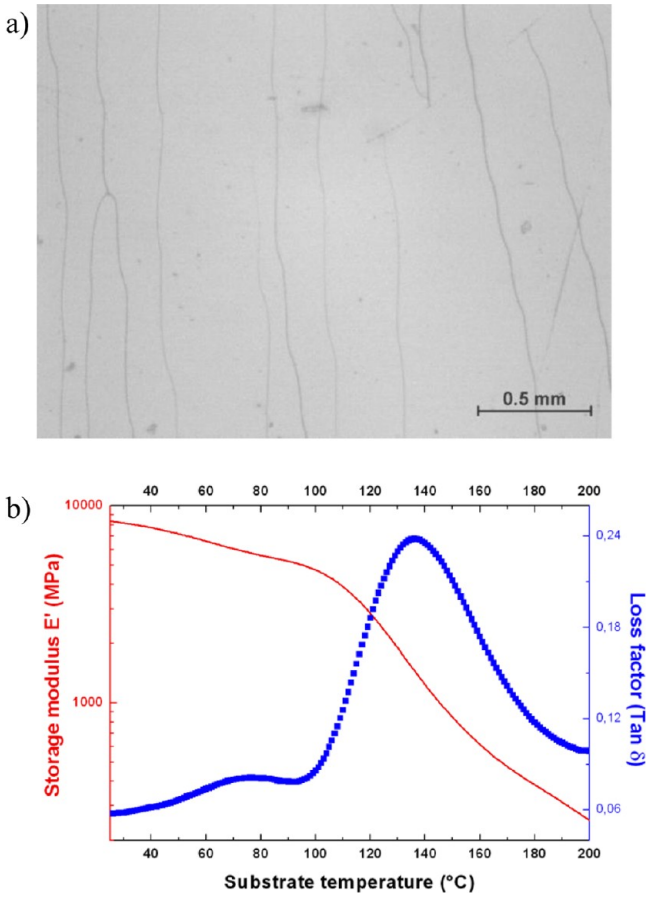

Figure 10. (a) Micrograph picture captured after deposition at 110 °C and (b) analysis DMA of PEN substrate.

Therefore, DMA experiments are performed to evaluate the thermomechanical properties of PEN films. Result is given in Figure 10b. The storage modulus decreases as a function of temperature. A first transition appears with a decrease of storage modulus at 70 °C. This is confirmed by loss factor curve. This transition corresponds to the β^* relaxation assigned to the motion of the naphthalene rings.[55,56] Despite this molecular relaxation, barrier performance is good in the range 70−90 °C, which certainly means that PEN stretching is not high enough to trigger cracking. A second transition is detected at higher temperature (113 °C), which is related to α relaxation corresponding to the glass transition of PEN. This relaxation induces a strong decrease of the storage modulus. After deposition step, coated PEN is unloaded and cools to room temperature, which triggers an additional compressive stress in the coating. This probably explains cracking as observed here, although mechanical resistance of the coating is expected to increase with temperature according to scratch results.

The link between structure and permeability of layers described in this work allows to develop layers with controlled properties. It was shown from the same authors that deposition of alternate $SiO_xH_y/SiO_xC_yN_zH_w$ multilayers further increase barrier properties compared to SiO_xH_y monolayer.[13] This work shows that deposition at higher temperature leads to SiO_xH_y layers with better oxygen barrier properties and $SiO_xC_yN_zH_w$ layers with smoother topography. Therefore deposition of alternate $SiO_xH_y/SiO_xC_yN_zH_w$ multilayers is considered as very promising when deposited at temperatures higher than room temperature, having in mind that BIF values higher than 1000 shall be obtained to address the less demanding applications of flexible electronics encapsulation.[8]

Furthermore, other improvements are expected from the development of a new roll-to-roll configuration or from choosing substrate with improved thermomechanical resistance, which both shall avoid occurrence of cracking at elevated temperature as observed in the present work.

4. CONCLUSION

Structure and properties of monolayers deposited from HMDSO are studied at different deposition temperature in a Townsend discharge at atmospheric pressure. Both silicalike and PDMS-like layers show a better homogeneity and a finer structure when temperature is increased above room temperature. In particular, silicalike layers are characterized by a denser Si−O−Si network and a lower concentration of OH groups as temperature increases. This leads to a significant improvement of scratch resistance at deposition temperature of 110 °C and higher.

Oxygen permeability decreases when temperature increases, because of this more homogeneous microstructure and molecular structure with fewer defects. However, no barrier effect is measured at temperatures higher than 90 °C, which may be explained by cracking of the coating owing to a larger stretching of the substrate film.

These investigations open the way to the deposition at higher temperature of alternated silicalike/PDMS-like multilayers for gas-barrier purpose. It is expected that multilayers processed at 90 °C could provide very high barrier property. Further improvement shall be obtained at even higher temperature if cracking of the coating could be avoided.

■ ASSOCIATED CONTENT

Supporting Information

Experimental setup drawing and supporting data about FTIR spectroscopy, XPS analysis, AFM measurements, and nanoscratch analysis. This material is available free of charge via the Internet at http://pubs.acs.org.

■ AUTHOR INFORMATION

Corresponding Author

*E-mail: nicolas.gherardi@laplace.univ-tlse.fr (N.G.); julien.bardon@tudor.lu (J.B.).

Notes

The authors declare no competing financial interest.

■ ACKNOWLEDGMENTS

The authors thank the Luxembourg funding organization "Fonds National de la Recherche" (FNR) for financial support through the FlexProtect project and the grant AFR PHD-08-047 (Julien Petersen).

■ REFERENCES

(1) *Silanes and Other Coupling Agents*;Mittal, K., Ed.; VSP (Brill): Leiden, The Netherlands, 2009; Vol. 5.

(2) Chou, T. P.; Chandrasekaran, C.; Limmer, S. J.; Seraji, S.; Wu, Y.; Forbess, M. J.; Nguyen, C.; Cao, G. Z. *J. Non-Cryst. Solids* **2001**, *290*, 153.

(3) Paulussen, S.; Rego, R.; Goossens, O.; Vangeneugden, D.; Rose, K. *J. Phys. D: Appl. Phys.* **2005**, *38*, 568.

(4) Verheyde, B.; Havermans, D.; Vanhulsel, A. *Plasma Process. Polym.* **2011**, *8*, 755−762.

(5) Maechler, L.; Sarra-Bourret, C.; Chevallier, P.; Gherardi, N.; Laroche, G. *Plasma Chem Plasma Process* **2011**, *31*, 175−187.

(6) Schneider, J.; Akbar, M. I.; Dutroncy, J.; Kiesler, D.; Leins, M.; Schulz, A.; Walker, M.; Schumacher, U.; Stroth, U. *Plasma Process. Polym.* **2009**, *6*, 700−704.

(7) Lewis, J. *Mater. Today* **2006**, *9* (4), 38−45.

(8) Lewis, J.; Weaver, M. *J. Sel. Top. Quant. Electron.* **2004**, *10* (1), 45−47.

(9) Dennler, G.; Lungenschmied, C.; Neugebauer, H.; Sariciftci, N. S.; Latrèche, M.; Czeremuszkin, G.; Wertheimer, M. R. *Thin Solid Films* **2006**, *511−512*, 349−353.

(10) Wagner, H. E.; Brandenburg, R.; Kozlov, K. V.; Sonnenfeld, A.; Michel, P.; Behnke, J. F. *Vacuum* **2003**, *71*, 417.

(11) Alexandrov, S. E.; Hitchman, M. L. *Chem. Vap. Deposition* **2005**, *11*, 457−468.

(12) O'Neill, L.; O'Hare, L.-A.; Leadley, S. R.; Goodwin, A. J. *Chem. Vap. Deposition* **2005**, *11*, 477−479.

(13) Gherardi, N.; Maechler, L.; Sarra-Bournet, C.; Naudé, N.; Massines, F. In *Proceedings of the International Symposium on Plasma Chemistry*; Bochum, Germany, July 26−31, 2009 ; von Keudell, A., Winter, J., Böke, M., Schul-von der Gathen, V.; International Plasma Chemistry Society, 2009; http://www.ispc-conference.org/ispcproc/papers/804.pdf.

(14) Premkumar, P. A.; Starostin, S. A.; Creatore, M.; de Vries, H.; Paffen, R. M. J.; Koenraad, P. M.; van de Sanden, M. C. M. *Plasma Process. Polym.* **2010**, *7*, 635−639.

(15) Walker, M.; Meermann, F.; Schneider, J.; Bazzoun, K.; Feichtinger, J.; Schulz, A.; Krueger, J.; Schumacher, U. *Surf. Coat. Technol.* **2005**, *200*, 947−952.

(16) Schneider, J.; Kiesler, D.; Leins, M.; Schulz, A.; Walker, M.; Schumacher, U.; Stroth, U. *Plasma Process. Polym.* **2007**, *4*, 155−159.

(17) Petersen, J.; Bechara, R.; Bardon, J.; Fouquet, T.; Ziarelli, F.; Daheron, L.; Ball, V.; Toniazzo, V.; Michel, M.; Dinia, A.; Ruch, D. *Plasma Process. Polym.* **2011**, *8*, 895−903.

(18) Creatore, M.; Palumbo, F.; d'Agostino, R.; Fayet, P. *Surf. Coat. Technol.* **2001**, *142−144*, 163−168.

(19) Coclite, A. M.; Milella, A.; d'Agostino, R.; Palumbo, F. *Surf. Coat. Technol.* **2010**, *204*, 4012−4010.

(20) Leterrier, Y. *Prog. Mater. Sci.* **2003**, *48*, 1−55.

(21) Haque, M. S.; Naseem, H. A.; Brown, W. D. *Thin Solid Films* **1997**, *308−309*, 68−73.

(22) Pecheur, A.; Autran, J. L.; Lazarri, J. P.; Pinard, P. *J. Non-Cryst. Solids* **1999**, *245*, 20−26.

(23) Ojeda, F.; Montero, I.; Abel, F.; Albella, J. M. *Chem. Mater.* **2001**, *13*, 3986−3992.

(24) Sahli, S.; Rebiai, S.; Raynaud, P.; Segui, Y.; Zenasni, A.; Mouissat, S. *Plasmas Polym.* **2002**, *7* (4), 327−340.

(25) Trunec, D.; Zajíčková, L.; Buršíková, V.; Studnička, F.; Stahel, P.; Prysiazhnyi, V.; Peřina, V.; Houdková, J.; Navrátil, Z.; Franta, D. *J. Phys. D: Appl. Phys.* **2010**, *43*, 225403.

(26) Schaefer, J.; Foest, R.; Quade, A.; Ohl, A.; Meichsner, J.; Weltmann, K. D. *Eur. Phys. J. D* **2009**, *54*, 211−217.

(27) Landreau, X.; Dublanche-Tixier, C.; Jaoul, C.; Le Niniven, C.; Lory, N.; Tristant, P. *Surf. Coat. Technol.* **2011**, *205*, 335−341.

(28) Landreau, X; Lanfant, B; Merle, T; Dublanche − Tixier, C.; Tristant, P. *Eur. Phys. J. D.* **2012**, *66*, 160.

(29) Creatore, M.; Cigal, J.-C.; Kroesen, G. M. W.; van de Sanden, M. C. M. *Thin Solid Films* **2005**, *484*, 104−112.

(30) Deshmukh, S. C.; Aydil, E. S. *J. Vac. Sci. Technol.* **1995**, *13*, 2355−2367.

(31) Massines, F.; Gherardi, N.; Fornelli, A.; Martin, S. *Surf. Coat. Technol.* **2005**, *200*, 1855−1861.

(32) Enache, I.; Caquineau, H.; Gherardi, N.; Paulmier, T.; Maechler, L.; Massines, F. *Plasma Process. Polym.* **2007**, *4*, 806−814.

(33) Premkumar, P. A.; Starostin, S. A.; de Vries, H.; Paffen, R. M. J.; Creatore, M.; Eijkemans, T. J.; Koenraad, P. M.; van de Sanden, M. C. M. *Plasma Process. Polym.* **2009**, *6*, 693−702.

(34) Maechler, L.; Cioarec, C.; Enache, I.; Naudé, N.; Caquineau, H.; Massines, F.; Gherardi, N. In *Proceedings of the 54th Annual Technical Conference*; Chicagom April 16−21, 2011 ; Society of Vacuum Coaters: Albuquerque, NM, 2011.

(35) Mahieu, S.; Ghekiere, P.; Depla, D.; De Gryse, R. *Thin Solid Films* **2006**, *515*, 1229.

(36) Lisovskii, I. P.; Litovchenko, V. G.; Lozinskii, V. G.; Steblovskii, G. I. *Thin Solid Films* **1992**, *213*, 164−169.

(37) Gunde, M. K. *Physica B* **2000**, *292*, 286−295.

(38) Supiot, P.; Vivien, C.; Granier, A.; Bousquet, A.; Mackova, A.; Escaich, D.; Clergereaux, R.; Raynaud, P.; Stryhal, Z.; Pavlik, J. *Plasma Process. Polym.* **2006**, *3*, 100−109.

(39) Yang, C. S.; Yu, Y. H.; Lee, K. M.; Lee, H. J.; Choi, C. K. *Thin Solid Films* **2003**, *435*, 165−169.

(40) Chou, J. S.; Lee, S. C. *J. Appl. Phys.* **1995**, *77*, 1805−1807.

(41) Zhao, Y.-P.; Drotar, J. T.; Wang, G.-C.; Lu, T.-M. *Phys. Rev. Lett.* **2001**, *87* (13), 136102.

(42) Brunet-Bruneau, A; Rivory, J.; Rafin, B; Robic, J. Y.; Chaton, P. *J. Appl. Phys.* **1997**, *82*, 1330−1335.

(43) Efimov, A. M.; Pogareva, V. *Chem. Geol.* **2006**, *229*, 198−217.

(44) Schäfer, J; Horn, S.; Foest, R; Brandenburg, R; Vasina, P.; Weltmann, K. D. *Surf. Coat. Technol.* **2011**, *205*, S330−S334.

(45) Milella, A; Creatore, M.; Blauw, M. A.; van de Sanden, M. C. M. *Plasma Process. Polym.* **2007**, *4*, 621−628.

(46) Davis, K. M.; Tomozawa, M. *J. Non-Cryst. Solids* **1996**, *201*, 177−198.

(47) Han, S. M.; Aydil, E. S. *Thin Solid Films* **1996**, *290−291*, 427−434.

(48) Pai, P. G.; Chao, S. S.; Takagi, Y.; Lucovsky, G. *J. Vac. Sci. Technol., A* **1986**, *4*, 689−695.

(49) Kirk, C. T. *Phys. Rev. B* **1988**, *38*, 1255−1273.

(50) Raballand, V.; Benedikt, J.; von Keudell, A. *Appl. Phys. Lett.* **2008**, *92*, 091502.

(51) Neuhauser, M.; Barwulf, S.; Hilgers, H.; Lugscheider, E.; Riester., M. *Surf. Coat. Technol.* **1999**, *119*, 981−985.

(52) Fahlteich, J.; Fahland, M.; Schönberger, W.; Schiller, N. *Thin Solid Films* **2009**, *517*, 3075−3080.

(53) Deilmann, M.; Grabowski, M.; Theiß, S.; Bibinov, N.; Awakowicz, P. *J. Phys. D: Appl. Phys.* **2008**, *41*, 135207.
(54) Körner, L.; Sonnenfeld, A.; Rudolf von Rohr, Ph. *Thin Solid Films* **2010**, *518*, 4840−4846.
(55) Mackintosh, A. R.; Liggat, J. J. *J. Appl. Polym. Sci.* **2004**, *92*, 2791−2796.
(56) Chen, D.; Zachmann, H. G. *Polymer* **1991**, *32*, 1612−1621.